This is the pre-peer reviewed version of the following article:
T. Katase, H. Takahashi, T. Tohei, Y. Suzuki, M. Yamanouchi, Y. Ikuhara, I. Terasaki and H. Ohta, Advanced Electronic Materials 1, 1500199 (2015)., which has been published in final form at http://onlinelibrary.wiley.com/wol1/doi/10.1002/aelm.201500199/abstract.

Solid-phase epitaxial growth of A-site-ordered perovskite $Sr_{4-x}Er_xCo_4O_{12-\delta}$: a room temperature ferrimagnetic p-type semiconductor

Takayoshi Katase[1,*], Hidefumi Takahashi[2], Tetsuya Tohei[3], Yuki Suzuki[1], Michihiko Yamanouchi[1], Yuichi Ikuhara[3], Ichiro Terasaki[2,*] and Hiromichi Ohta[1,*]

[1]Research Institute for Electronic Science, Hokkaido University, N20W10, Kita-ku, Sapporo 001-0020, Japan

[2]Department of Physics, Nagoya University, Chikusa-ku, Nagoya 464-8602, Japan

[3]Institute of Engineering Innovation, The University of Tokyo, 2-11-16 Yayoi, Bunkyo-ku, Tokyo 113-8656, Japan

[*]E-mail: katase@es.hokudai.ac.jp, tera@cc.nagoya-u.ac.jp , hiromichi.ohta@es.hokudai.ac.jp

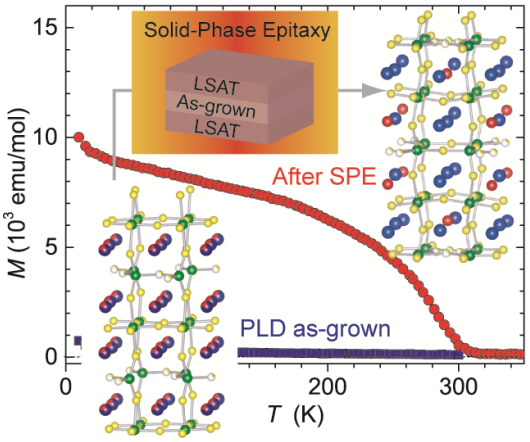

Solid-phase epitaxial growth of A-site-ordered perovskite $Sr_{4-x}Er_xCo_4O_{12-\delta}$ (SECO), a room temperature ferrimagnetic p-type semiconductor, is demonstrated. The A-site ordered SECO film with p-type semiconductivity exhibits anomalous Hall effect at room temperature, which is promising for the development of heterojunction devices of spintronics.

Keywords: ordered perovskite, cobaltite, epitaxial film, ferrimagnetic semiconductor

Abstract

The oxygen-deficient $Sr_{4-x}Er_xCo_4O_{12-\delta}$ (SECO), one of the ordered perovskite oxides, is a room-temperature (RT) ferrimagnetic semiconductor that arises from the A-site-ordered structure. Development of such material could lead to the realization of spintronic heterojunction devices; however, to this point there have been difficulties in achieving the A-site-ordered structure in SECO thin film. Here, we demonstrate single-crystalline film growth of SECO with perfectly aligned A-site-ordered structure on $(LaAlO_3)_{0.3}(Sr_2TaAlO_6)_{0.7}$ substrates by solid-phase epitaxy (SPE) method. The brownmillerite-type, A-site-disordered structure of the as-grown epitaxial film clearly changes into well-aligned A-site-ordered structure after heat treatment at 1050 °C in air; the aligned ordered structure in the film is clearly visualized at atmic level. This ordering induces ferrimagnetism with Curie temperature (T_c) ~310 K and it is found that the SECO film with p-type semiconductivity exhibits anomalous Hall effect at the temperature up to 300 K, which is suitable for the test bench to demonstrate advanced spintronic heterojunction devices, operating at RT. The present SPE method is expected to serve as a powerful technique for the fabrication of thin films and exploration of potential characteristics of A-site-ordered perovskite oxides.

1. Introduction

Perovskite transition-metal oxides are the most important family of materials to show a wide range of quantum phenomena including superconductivity,[1] colossal magnetoresistance,[2] and itinerant ferromagnetism,[3] among others. Due to the flexibility in the perovskite structure, introducing additional elements into the A or B sites of the perovskites (general chemical formula ABO_3) often results in ordered perovskite structure.[4] Since the self-assembled ordered structure stabilizes long-range order due to the absence of random Coulomb potential,[5] it is commonly found that this ordering leads to a large increase in phase transition temperatures and enriches competing electronic phases,[6] giving rise to specific properties not inherent to normal (randomly disordered) perovskites.

An important example is the oxygen-deficient perovskite cobaltite, $Sr_{4-x}R_xCo_4O_{12-\delta}$ (S*R*CO, where *R* is Y or rare earth elements such as Dy, Ho, and Er), possessing an A-site-ordered structure. S*R*CO is a ferrimagnetic semiconductor with Curie temperature (T_c) of 335 K,[7] which is considerably higher than those of the perovskite cobaltites without ordered structure, such as (La,Sr)CoO_3[8] and $SrCoO_3$ ferromagnetic metals.[9,10] The S*R*CO has a tetragonal crystal structure with the space group *I*4/*mmm*. The A-site cations (Sr^{2+} and R^{3+}) are ordered within the *ab*-plane and two types of perovskite layers, CoO_6 and oxygen-deficient $CoO_{4.25}$, alternate along the *c*-axis such that oxygen ions are regularly deficient (oxygen vacancies are ordered) around the *R*−*R* bond.[11] Although there is currently no consensus on the mechanism of high-T_c ferrimagnetism in S*R*CO due to the variety of spin states in Co ions with formal valence of +3 for S*R*CO,[7,12,13] the most widely accepted explanation is that ferrimagnetism comes from the spin-state ordering of Co ions with a collinear G-type antiferromagnetic structure — this arises as the Co ions with different oxygen coordination possess different magnetic moments and the spin state becomes order under the influence of A-site ordered

structure; therefore, the complex ordered structure plays a key role in achieving RT ferrimagnetic S*R*CO.

In particular, the A-site-ordered S*R*CO can be expected as a promising magnetic material for spintronics application, where semiconductor spintronics using ferro(/ferri)magnetic oxides with T_c over RT are one of the hottest topics.[14] The most striking feature of S*R*CO is that they are RT p-type ferrimagnetic semiconductor, whereas the majority of magnetic semiconductors of perovskite oxides tend to exhibit n-type conductivity.[14] To the best of our knowledge, only the exception of p-type ferro(/ferri)magnetic semiconductor with T_c over RT is B-site-ordered La_2NiMnO_6;[15] there are few candidates for p-type magnetic semiconductors of perovskite oxides.[16] Advances in the epitaxy of perovskite oxides make it possible to realize magnetic p-n junction devices and/or bipolar transistors with all-perovskite heterostructures, which enables spintronic devices, such as magnetic sensing, nonvolatile memory, and reprogrammable logic, using depletion layer at the interface.[17] To this point, application-relevant characteristics of S*R*CO such as its spin transport properties have yet to be investigated experimentally.

The synthesis of thin-films of S*R*CO with a well-aligned, ordered structure is highly desirable not only for the investigation of the material's intrinsic electromagnetic properties, but also to evaluate its suitability for advanced spintronic device applications. However, growth of this material has proved challenging due to the difficulties in making the aligned A-site-ordered structure. Generally, the high-temperature vapor-phase epitaxy (VPE) is appropriate for growth of single-crystalline film of perovskite materials,[18] but conventional VPE process cannot be employed because the A-site-cation ordering temperature is very high (≥ 1000 °C),[19] which may lead to sublimation of the constituents and, consequently, a non-stoichiometric product because of the high vapor pressure of Sr- and Co-related species.

In our preliminary experiments by VPE process, the severe sublimation of film was observed at growth temperature ≥ 850 °C, as will be mentioned in this paper. On the other hand, for synthesis of bulk single-crystals of S*R*CO by solid-phase growth, multi-domain structures have tended to crystallize instead of the aligned A-site-ordered structure.[20]

To overcome this problem, we propose a solid-phase epitaxy (SPE) for the growth of S*R*CO single-crystalline thin-films, which would be appropriate method to achieve well-aligned A-site-ordered structure in perovskite oxides. The SPE method is comprised of a two-step film-synthesis process that combines low-temperature epitaxial growth and high-temperature heat treatment. **Figure 1** depicts the synthesis strategy for A-site-ordered perovskites by considering the ordering temperatures of A-site cations and oxygen vacancies. In order to evaluate the A-site ordering in S*R*CO, Er was selected as the *R* component to assist in structural characterization as the difference in atomic number between Sr and Er is much greater than that between Sr and Y; this allows for much clearer differentiation between the elements in X-ray and electron diffraction studies.

In the first step of $Sr_{4-x}Er_xCo_4O_{12-\delta}$ (SECO) growth, a film with a brownmillerite (BM)-type structure (shown in **Figure 1(a)**), *i.e.*, A-site-disordered perovskite framework with oxygen-vacancy order,[21] was deposited on a mixed-perovskite $(LaAlO_3)_{0.3}(Sr_2TaAlO_6)_{0.7}$ (LSAT) substrate.[22] The epitaxial growth of this BM-structured film is considered to be more straightforward than for the A-site-ordered structure due to the much lower ordering temperature[23]; moreover, the epitaxial growth of un-doped $SrCoO_{2.5}$ with a similar BM-type structure films on LSAT substrates has been widely reported.[24] Then, in order to induce A-site ordering, high-*T* annealing was performed on the as-grown film in air, with the expectation that the A-site cations of Sr and Er would form a well-aligned, ordered structure

(shown in **Figure 1(b)**) along with oxygen-vacancy-order rearrangement due to the large differences in their ionic radii,[25] reflecting the epitaxial crystal lattices of SECO film.

Here, we report the epitaxial growth of A-site-ordered perovskite SECO by SPE method and investigate its electromagnetic properties using the thin films. It is found that the BM-type structure of the as-grown epitaxial film converts to the well-aligned A-site-ordered structure via heat treatment at 1050 °C in air, yielding ferrimagnetism with a T_c of ~310 K. This is the first report on the single-crystalline film of A-site-ordered perovskites, where the well-aligned ordered structure is clearly resolved at atmic level. Our SPE process is effective to grow A-site-ordered perovskite thin films, which advances the fundamental understanding of their intrinsic properties and application characteristics.

2. Results and Discussions

2.1. Solid-Phase Epitaxy

The SPE method is composed of following steps.[26] Step 1: SECO (nominal x = 0.4) films (80-nm-thick) were deposited on (001) LSAT substrates by pulsed laser deposition (PLD) at optimized growth temperature (T_g) of 820 °C under an oxygen pressure (P_{O2}) of 10 Pa [see Supporting Information **Figure S1** for growth phase diagram of SECO films as a function of T_g and P_{O2}]. A KrF excimer laser with energy fluence of ~2 J cm^{-2} pulse^{-1} and repetition rate of 10 Hz was used to ablate a ceramic target of $Sr_{3.6}Er_{0.4}Co_4O_{12-\delta}$. After film deposition at a rate of approximately 5.3 nm min^{-1}, the films were cooled to RT under the same P_{O2}. Step 2: The as-deposited SECO film was fully overlaid by another LSAT plate (10×10×0.5 mm^3) to prevent the sublimation of the constituent in the film during the heat treatment in step 3. Step 3: The film was heated at temperature (T_a) of 1050 °C for 40 h in air [see Supporting Information **Figure S2** for crystal-structure change of SECO films as a function of T_a]. After

the heat treatment, the film was cooled down to RT in the furnace. Finally, the LSAT plate was removed. The resultant film surface looked very clean; no chemical reaction with the LSAT plate was observed.

2.2. Structural analyses

Figure 2(a) shows out-of-plane X-ray diffraction (XRD) pattern of the SPE-grown SECO film together with that of as-grown film for comparison. The diffraction peaks for both films can be assigned to the 00*l* SECO along with those of the LSAT substrates; no impurity peaks are observed. The double lattice spacing along the *c*-axis (*l* = 2, 6, 10) originates from the oxygen-vacancy-ordered structure, which indicate that oxygen-vacancy ordering in both films is well-aligned along *c*-axis as shown in Fig.1 a and b;[21] moreover, the perovskite-structure framework is shown to remain after the SPE process. The elemental ratios of these films were found to be Sr : Er : Co = 0.89 : 0.11 : 1.00, as characterized by electron probe microanalyser, consistent with the nominal composition ($Sr_{3.6}Er_{0.4}Co_4O_{12-\delta}$) of the ceramic target. In addition, we have confirmed that the compositions of each element (Sr, Er, Co) were homogeneous and there is no segregation of secondary phase on film surface. These results demonstrate that the SPE process does not lead to loss of material through sublimation.

Since the oxygen-vacancy ordering makes the superstructure peaks along *c*-axis (*l* = 2, 6, 10) regardless of whether A-site cations are ordered or not, it is impossible to evaluate the A-site ordering in the SPE-grown SECO film by the symmetric diffraction measurements. In order to evaluate the A-site-cation (Sr/Er) ordering in the film, ϕ scans of the asymmetric 103 diffraction spot for the structure of A-site-ordered SECO were carried out, because the structural factor of *F*(103) (*l* = 3*h*) increases significantly on transition to an A-site-ordered structure,[11] where it should be noted that the A-site ordering in bulks has been generally

evaluated by the appearance of 103 diffraction spot.[7] **Figure 2(b)** shows the ϕ-patterns of the 103 diffraction spot for SPE-grown SECO films. The measurement on the SPE-grown film yields four distinct peaks with 90° rotational intervals, suggesting that the SPE process induces a transition to A-site ordering in the SECO epitaxial films. **Figure 2(c)** shows reciprocal space mapping (RSM) of the SPE-grown SECO film. Intense diffraction spots from the 20$\underline{12}$ SECO and LSAT substrate are observed with an identical in-plane lattice constant of 0.387 nm, indicating a coherent epitaxial growth of SECO occurred on the LSAT substrate without lattice relaxation. These results indicate that the SPE process produces an epitaxial film with a well-aligned, A-site-ordered structure, keeping a perovskite framework.

Figure 2(d) shows topographic atomic force microscopy (AFM) image of the SPE-grown SECO film. A cross-sectional line profile (red line) across the AFM image shows the presence of a clear stepped-and-terraced surface of the film. Square-shaped domain structures reflecting the tetragonal crystal lattice of SECO are observed along the step edge with a height of ~0.4 nm, a value roughly equivalent to a quarter-length of the *c*-axis of SECO (*i.e.*, the unit cell of primitive perovskite structure). This atomically flat surface, also confirmed in reflection high-energy electron diffraction (RHEED) patterns from the intense diffraction spots shown in the inset of **Figure 2(d)**, conveys that the SPE-grown SECO film is of sufficiently high quality for application in the test bench to demonstrate heterojunction devices. It should be also noted that there are diffraction intensity and modulation in between the primary ones of perovskite structure in the RHEED pattern. As it reflects the surface atomic structure, the existence of weak diffraction spots originates from the superstructure (ordered structure) of film surface and/or surface reconstruction. Meanwhile, for as-grown SECO film, the additional diffraction spots were not observed in RHEED pattern (See Supporting Information **Fig. S3** for the AFM image and RHEED pattern of as-grown SECO

film), suggesting that the diffraction intensity modulation observed in SPE-grown film should relate with the A-site-ordered structure.

As mentioned above briefly, the XRD patterns of the SECO films shown in this study were derived from films grown under optimized conditions. In optimizing the growth process, it was found that the highly pure, oxygen-vacancy-ordered (BM-type) SECO structure could only be obtained within a very narrow growth window; we posit that this is related to the energetically favorable low oxidation state of the Co ion in addition to the high vapor pressure of Sr- and Co-related species under the typical PLD process. This hypothesis is supported by the observation that i) the CoO impurity formed under reducing conditions ($P_{O2} < 1$ Pa) and ii) sublimation of the constituents from the surface was observed at high $T_g \geq 850$ °C rendering one-step; high-temperature growth of this material was impossible by this PLD process. In addition, the A-site ordering was shown to depend strongly on T_a; the 103 diffraction peaks corresponding to the A-site-ordered structure appeared at $T_a \geq 950$ °C and grew in intensity with increases of T_a up to 1050 °C. A systematic study on growth and annealing conditions for SECO films was undertaken, with the results summarized in Supporting Information **Figs. S1** and **S2**, respectively. In addition, it should be noted from the XRD patterns in **Fig. 2(a)** that the positions of out-of-plane diffraction peaks shift to higher q after SPE process, corresponding to a contraction in the c-axis lattice parameter (from 1.555 nm to 1.528 nm). As shown in **Fig. S3**, the lattice shrinkage occurs concurrently with the transition to A-site ordering at $T_a \geq 950$ °C. The most plausible reason for the shrinkage of c-axis lattice parameter is the transition to A-site-ordered structure with the distortion of BO_6 octahedron and O-Co-O chains in perovskite structure along c-axis, as illustrated in Fig.1. It is well known that the overall unit cell volume of ABO_3 perovskite is sensitive to the size and shape of the BO_6 octahedron,[27] given that these structural units constitute the framework of the perovskite structure. Therefore, it can be deduced from this c-axis lattice shrinkage that the

BO_6 octahedra undergo structural distortion on A-site ordering. It should be noted that there is a possibility of the oxygen content change with high temperature annealing, but it can be considered that there is little change in the oxygen content, due to the experimental fact that the conductivity remained almost unchanged after the post-growth annealing (as will be shown in electronic-property characterization section). Although we cannot perfectly rule out the change of oxygen content in SECO film through SPE process, the transition to A-site-ordered structure is the most plausible origin of the *c*-axis lattice shrinkage.

To further visualize the ordered structure in the SPE-grown SECO films, microstructure analysis was carried out with the aid of spherical aberration-corrected scanning transmission electron microscopy (STEM). **Figures 3(a)** shows a selected-area electron diffraction (SAD) pattern of the SPE-grown SECO epitaxial film. For comparison, the SAD pattern of as-grown SECO film is shown in Supporting Information **Fig. S4(a)**. The brighter diffraction spots are assigned to the primitive cubic perovskite structure. For the SAD pattern of as-grown film (Fig. S4(a)), additional reflections, represented by arrows, are present just between the principal spots of perovskite structure, which is consistent with oxygen-vacancy-ordered BM-type structure.[25] Comparing the SAD patterns between SPE-grown and as-grown SECO film, the further additional weaker diffraction spots of (*h* 0 *l*), where *h* and *l* are odd numbers, are shown to be present in SPE-grown SECO film; these can be well explained by the appearance of A-site-ordered structure in SECO film.[11]

Figure 3(b) shows a Z-contrast, high-angle annular dark-field (HAADF) STEM image of the SPE-grown SECO epitaxial film on LSAT substrate. The cross-sectional image clearly displays that a sharp interface exists between SECO and LSAT; this is clearly visible due to the difference in contrast between the two materials, arising from the heavier constituent atoms of the LSAT substrate (Z_{La} = 57 and Z_{Ta} = 73) compared to the SECO film (Z_{Sr} = 38,

Z_{Co} = 27). The atomic arrangement is smoothly connected from the LSAT substrate to the SPE-grown SECO film, which confirms the film epitaxy at the interface and is consistent with the RSM shown in **Fig. 2(c**).

Magnified views of the SPE-grown SECO film are presented in **Fig. 3(c) and (d)**: **(c)** is a HAADF-STEM image; **(d)** an annular bright-field (ABF)-STEM image.[28] These images were respectively obtained by averaging 20 original HAADF and ABF images, taken from each image scanned in wide range. Simultaneous HAADF and ABF imaging allows us to visualize the precise positions of all constituent atoms, including oxygen. The intensity in HAADF image is roughly proportinalto Z^2, which results in easier visualiztion of heavy elements, whereas in ABF image, the constituent atoms are observed as dark contrast and lightweight elements can be clearly seen, (*i.e.*, regions containing lighter elements provide lighter contrast) allowing for visual inspection of oxygen columns. **Figure** 3**(e)** is a schematic illustration of corresponding crystal structure of A-site ordered SECO for evaluating the atomic structure seen in these images.

In the HAADF-STEM image (**Fig. 3(c)**), A-site-cation columns form a periodic square spots pattern, and each square is centered with weaker spot that corresponds to the Co column structure. The intensity of the A-site-cation spots change periodically; the brighter spots (corresponding to mixed columns of Sr (Z = 38) and Er (Z =68)) alternate with less bright spots produced by the pure Sr columns forming a chess-board pattern; this is consistent with the predicted atomic structure of the ordered SECO shown in **Fig. 3(e)**. The ordered alternation of the (Sr, Er) and Sr columns is clearly seen in the HAADF intensity line profile (shown in the panel below **Fig. 3(c)**), which was measured along the white line drawn across the A-site-cation spots [see Supporting Information **Figure S5** for the detailed analysis for the line profiles of the HAADF-STEM image]. On the other hand, in the ABF-STEM image (**Fig. 3(d)**), along with the darker spots of the cation columns, pure oxygen columns are visible as

weak dark spots at the positions characteristic for the perovskite structure. The ordered alternation of the filled and deficient oxygen columns is clearly seen in the ABF intensity profile (shown in the panel below **Fig. 3(d)**), taken along the CoO row. In addition, it should be noted that the elongated spots observed at mixed columns of Sr and Er in the magnified HAADF image (Fig.3(c)) also suggest the A-site-cation ordering in the SECO film, as is shown in the simulated crystal structure of A-site-cation ordered SECO (Fig. 3(e)). These results clearly support that the SPE-grown SECO film has a well aligned ordered structure of both the A-site cation and oxygen vacancy components. For comparison, the ABF-STEM images of as-grown SECO film are shown in Supporting Information Fig. S4(b) and (c). The observed atomic structure is consistent with the crystal structure of A-site-disordered SECO with BM-type structure (Fig. S4(b)). The ABF intensity profile, shown in the botom pannel of Fig. S4(c), represents that the intensity of A-site-cation spots is almost constant, indicating the A-site-disordered structure. These results clearly support that the as-grown film is BM-type structure and the crystal structure changes from A-site-disordered to A-site-ordered structure in SECO film.

2.3. Electromagnetic properties

The electromagnetic properties of both as-deposited and SPE-grown SECO epitaxial films were subsequently probed to investigate the effect of A-site ordering on the material's functional properties. **Figure 4(a)** shows the temperature dependence of magnetization (*M*–*T*) under a magnetic field (*H*) of 20 Oe after zero-field cooling, where *H* was applied parallel to the in-plane direction. While the magnetic signal was measured to be considerably small for the as-deposited SECO film, the SPE-grown SECO film exhibited a much larger degree of magnetization; this is shown in Supporting Information **Figure S6** that plots the change in *M*–*T* curves for SPE-grown SECO films treated with different T_a. The *M*–*T* curves were observed to systematically change for different films annealed in the T_a range 850–1050 °C,

and a dramatic increase in the magnitude of magnetization was observed for films with $T_a \geq$ 950 °C, providing a strong correlation between the observed magnetization and the A-site ordering. The T_c for SPE-grown SECO film at T_a = 1050 °C is estimated to be ~310 K, which is slightly lower than a reported value (335 K) of A-site-ordered bulk polycrystals.[7] This discrepancy in T_c is presumed to originate from lattice distortion in the SECO thin films; it has been reported that a slight compressive strain can significantly decrease T_c of bulk due to a spin-state transition from a high- to low-spin state.[29] By comparing the lattice parameters of S*R*CO bulk (*R* = Y) with T_c = 335 K (a = 0.7674 nm (a/2 = 0.3837 nm) and c = 1.534 nm (c/4 = 0.3835 nm))[7] with those obtained for the SPE-grown SECO thin films (a = 0.7740 nm (a/2 = 0.3870 nm) and c = 1.528 nm (c/4 = 0.3820 nm)) in this work, it can be shown that epitaxial strain from the LSAT substrate shrinks and expands the out-of-plane and in-plane lattice constants of the SECO film respectively (**Fig. 2**), which would account for the decrease of T_c to 310 K. However, modulation of the T_c to higher values via epitaxial strain could be relatively straightforward, given that the degree of lattice distortion can be controlled by choosing perovskite substrates with different lattice parameters. A magnetic hysteresis loop of the SPE-grown SECO film at 10 K is shown in the inset of **Fig. 4(a)**; this film clearly exhibits ferromagnetic behavior. A small *H*-linear component is observed in the high *H* region that is attributed due to paramagnetic spins of Er^{3+} and/or field-induced polarization. By subtracting the small *H*-linear component, the saturation moment of ~0.29 μ_B/Co (μ_B is a Bohr magneton) is comparable with a value of 0.25 μ_B/Co obtained for A-site ordered bulk polycrystals at the same temperature and indicates that the SPE-grown SECO film exhibits bulk ferrimagnetic behavior.[7] These results confirm that A-site ordering induces ferrimagnetic order with a T_c of 310 K in the SPE-grown SECO epitaxial films.

Figure 4(b) shows the temperature dependence of electrical conductivity (σ) in the SECO films. The σ of both as-deposited and SPE-grown SECO films increases as the temperature

increases, suggesting that the electronic transport follows a thermally activated behavior, where the transport properties should be dominated by doped holes on the minority low-spin Co^{4+} ion in the high-spin Co^{3+} matrix, possibly coming from non-stoichiometry of oxygen.[7] It shows that the σ does not follow a simple Arrhenius Law, *i.e.*, a linear relation between ln σ and T^{-1}. Instead, the σ–T curves for both thin-films appear to follow a ln σ–$T^{-1/4}$ law (shown in the inset). This behavior is often attributed to a variable-range hopping mechanism,[30] suggesting that the charge carriers in the SECO films tend to localize at temperatures ≤ 350 K. As shown by thermopower (S) measurements carried out at RT (**Fig. 4(c)**), S-values obtained from the slope of ΔV–ΔT plots are positive, indicating that both the SECO films are p-type semiconductor. Different S-values were observed for as-deposited and SPE-grown SECO films; in the former, a value of +176 μV K^{-1} was recorded, falling to +83 μV K^{-1} after SPE-process. Since no corresponding change in σ was observed (**Fig. 4(b)**), the decrease of S-values is attributed to the A-site structural ordering rather than changes in carrier concentration (*i.e.* carrier doping by the reduction of oxygen vacancies); there seems to be little change in oxygen content during the heat treatment.[19] This can be understood in terms of an extended Heikes formula that includes contributions from the spin configuration[31]; this indicates that the S-values significantly decrease depending on the spin state (high or low) of the Co^{3+} ions in SECO. Based on the fact that the previously reported S-value of SECO bulk polycrystals (in the range from +90 to +100 μV K^{-1}) is close to those recorded in SPE-grown SECO film,[29] it can be deduced that the bulk ferrimagnetism exhibited by the SPE-grown film can be attributed to the presence of high-spin state Co^{3+} ions.

Here, we would like to discuss the oxygen content in the SECO films grown by SPE process, although it is difficult to quantitatively measure the oxygen content of the film. For bulk polycrystalline (Sr,R)$CoO_{3-\delta}$ exhibiting RT ferrimagnetism, the oxygen content, 3–δ, was

estimated to be 2.6, in which the Co valence is +3.[7] The A-site-cation ordering closely links with the oxygen-vacancy ordering in S*R*CO; A-site-cations become disorder, simultaneously with the disordering of oxygen vacancies as increase of oxygen content. Therefore, the controllability of oxygen content should be narrow for A-site-ordered SECO film and the observation of RT ferrimagnetism in the SECO film suggests that the oxygen content seems to be almost the same with that of bulks.

The anomalous Hall effect (AHE) is an important characteristic to provide evidence for spin-polarization of charge carriers that mediates ferromagnetic interaction between the localized spins of magnetic ions.[32,33] **Figure 4(d)** shows the *H*-dependence of transverse Hall resistivity (ρ_{xy}) of the SPE-grown SECO epitaxial film at various temperatures in the range 200–350 K. In general, ρ_{xy} of ferromagnetic materials is expressed as the sum of ordinary and anomalous parts of Hall resistivity, *i.e.*, $\rho_{xy} = R_0 \cdot \mu_0 \cdot H + R_s \cdot M$, where R_0 and R_s are the ordinary and anomalous Hall coefficients, respectively, μ_0 is vacuum permeability, and M is magnetization.[34] The ρ_{xy} curves clearly exhibit non-linear hysteresis loops with positive R_s, which provides evidence for coupling between the ferrimagnetism and charge carriers in the SPE-grown SECO film. The AHE is observed for $T \leq 300$ K, where the weak linear slope at high $H \sim 70$ kOe confirms that the AHE is dominant in the ρ_{xy} curves, but becomes negligible at 350 K (*i.e.*, in this region, ρ_{xy} increases linearly with H). Although there remains the possibility that AHE partially originates from magnetic impurities, such as Co nano-particle,[35] it is hard to consider that the segregation of Co metal impurity occurs after high-T annealing in air. Additional characterization, such as X-ray magnetic circular dichroism,[36] is necessary for further discussion, but the observed AHE suggest that the spin-polarized magnetic ordering remains at temperatures above RT.

To roughly estimate the carrier concentration (n) of the SECO film, R_0 is deduced from the linear slope of ρ_{xy} at high field around 70 kOe, where the anomalous Hall resistivity has already saturated [see Supporting Information **Fig. S7** for the analysis of Hall resistivity].[36] The R_0 is positive and becomes large at lower temperature. Considering that hole-doped Co^{4+} generally results in ferromagnetic conductor, whereas electron doped Co^{2+} basically results in magnetic insulator, the only one carrier type of hole is dominant in the transport property of the SECO film. The inset of **Fig. 4(d)** plots the n vs. T calculated from the equation of $n = (R_0 \cdot e)^{-1}$, where e is elementary charge. An increase in n observed from 5.8×10^{19} cm^{-3} at 200 K to 5.5×10^{20} cm^{-3} at 350 K is indicative of thermal activation of charge carriers.

In addition, the relation between anomalous Hall conductivity (σ_{AH}) and the longitudinal conductivity (σ_{xx}) for the SPE-grown SECO epitaxial film is summarized in Supporting Information **Fig. S8**. σ_{AH} and σ_{xx} are respectively deduced from $\rho_{AH} \cdot (\rho_{xx}^2 + \rho_{AH}^2)^{-1}$ and $\rho_{xx} \cdot (\rho_{xx}^2 + \rho_{AH}^2)^{-1}$, where ρ_{AH} is estimated by subtracting the linear background in ρ_{xy} at high H. The σ_{AH} increases with σ_{xx}, following the scaling line of proportional relation between σ_{AH} and $\sigma_{xx}^{1.6}$. The scaling relation agrees well with the theory for the low conductivity regime[37] and the behavior is consistent with that of other conventional oxide dilute magnetic semiconductors.[38] These results indicate that the SECO film behaves as a magnetic semiconductor at the temperature up to 300 K.

3. Conclusion

We have succeeded in fabricating single-crystalline films of SECO with A-site-ordered structure by a solid-phase epitaxy method. The A-site-disordered BM-type structure of the as-grown epitaxial film was observed to change into A-site-ordered structure on heat treatment at 1050 °C in air; the well aligned ordered structure is visually observed at atomic level. The

resulting thin-film was observed to possess ferrimagnetic order with a T_c of ~310 K. Although the T_c is relatively low due to epitaxial strain, it should be improved up to 370 K[13] by controlling the lattice distortion of the film, which make the film feasible for spintronic devices, operating at RT. It was found that the SPE-grown SECO film with p-type semiconductivity exhibits the anomalous Hall effect at temperatures up to 300 K, suggesting that the charge carriers in the films are spin polarized at RT. Further investigation into these SECO films is warranted in order to clarify the origin of the observed high-T_c ferrimagnetism; moreover, these films are promising as above-RT T_c p-type oxide magnetic semiconductor materials and are test bench suitable for exploring spintronic semiconductor heterojunction devices, operating at RT. The proposed SPE process is expected to serve as a powerful technique for the thin-film fabrication of the ordered perovskite materials, which can induce excellent electro-magnetic properties and advance their potential applications.

4. Experimental

Film-structure characterization: Crystal structures and orientation were investigated by high-resolution X-ray diffraction (anode radiation: monochromatic CuKα_1, ATX-G, Rigaku Co.). The film surface morphology was observed using Atomic Force Microscopy (Nanocute, Hitachi High-Tech). The film chemical compositions were characterized using a field-emission electron probe microanalyser (JXA-8530F, JEOL Ltd.). Cross-sectional thin-film samples for STEM observations were prepared by mechanical polishing and Ar^+ ion milling (PIPS) without using water. The cross-sectional microstructure and SAD pattern of the SECO film were examined by high-resolution STEM (JEM-ARM200F, JEOL Ltd.), where the electron incident direction was parallel to LSAT [010].

Electrical-transport and magnetic-property measurements: Electrical conductivity measurements were performed by the d.c. four-point probe method using Au electrodes. Thermopower was measured by giving a temperature gradient (ΔT) of ~4 K in the film using two Peltier devices, where the actual temperatures of both sides of SECO film surface were monitored by two tiny thermocouples.[39] Magnetic properties of SECO films with a sample size of 3 mm × 3 mm were measured by a superconducting quantum interference device magnetometer (SQUID, Quantum Design). *M*–*T* characteristics were measured after zero-field cooling, where the magnetic fields of 20 Oe was applied parallel to in-plane direction of the film after the magnetization at 30 kOe. Hall effect measurements were performed with a Physical Properties Measurement System (PPMS, Quantum Design) for SECO films with a channel size of 6.5 mm long and 3.0 mm wide. The electrical current was applied along the *ab*-plane of the film and the magnetic fields of up to 70 kOe were applied parallel to the *c*-axis.

Acknowledgements
We would like to thank Dr. Ryuji Okazaki for the valuable discussions. This work was in part supported by the Network Joint Research Center for Materials and Devices and Nanotechnology Platform Program (12024046) from MEXT. HO was supported by a Grant-in-Aid for Scientific Research on Innovative Areas (25106007) and KAKENHI for Scientific Research A (25246023) from JSPS. IT and HO were supported by JSPS KAKENHI for Scientific Research B (26287064). TK was supported by JSPS KAKENHI for Young Scientists A (15H05543). TT was supported by JSPS KAKENHI for Young Scientists B (24760533).

[1] R. J. Cava, B. Batlogg, J. J. Krajewski, R. Farrow, L. W. Rupp Jr, A. E. White, K. Short, W. F. Peck, T. Kometani, *Nature* **1988**, 332, 814–816.

[2] M. B. Salamon, M. Jaime, *Rev. Mod. Phys.* **2001**, 73, 583–628.

[3] G. Koster, L. Klein, W. Siemons, G. Rijnders, J. S. Dodge, C.-B. Eom, D. H. A. Blank, M. R. Beasley, *Rev. Mod. Phys.* **2012**, 84, 253–298.

[4] G. King, P. M. Woodward, *J. Mater. Chem.* **2010**, 20, 5785–5796.

[5] D. Akahoshi, M. Uchida, Y. Tomioka, T. Arima, Y. Matsui, Y. Tokura, *Phys. Rev. Lett.* **2003**, 90, 177203.

[6] T. Nakajima, H. Kageyama, H. Yoshizawa, K. Ohoyama, Y. Ueda, *J. Phys. Soc. Jpn.* **2003**, 72, 3237–3242.; A. A. Taskin, A. N. Lavrov, Y. Ando, *Phys. Rev. Lett.* **2002**, 90, 227201.

[7] W. Kobayashi, S. Ishiwata, I. Terasaki, M. Takano, I. Grigoraviciute, H. Yamauchi, M. Karppinen, *Phys. Rev. B* **2005**, 72, 104408.

[8] M. Kriener, C. Zobel, A. Reichl, J. Baier, M. Cwik, K. Berggold, H.Kierspel, O. Zabara, A. Freimuth, T. Lorenz, *Phys. Rev. B* **2004**, 69, 094417.

[9] T. Takeda, H. Watanabe, *J. Phys. Soc. Jpn.* **1972**, 33, 973–978.

[10] Y. Long, Y. Kaneko, S. Ishiwata, Y. Taguchi, Y. Tokura, *J. Phys. Condens. Matter.* **2011**, 23, 245601.

[11] S. Y. Istomin, J. Grins, G. Svensson, O. A. Drozhzhin, V. L. Kozhevnikov, E. V. Antipov, J. P. Attfield, *Chem. Mater.* **2003**, 15, 4012.

[12] D. V. Sheptyakov, V. Yu. Pomjakushin, O. A. Drozhzhin, S. Ya. Istomin, E. V. Antipov, I. A. Bobrikov, A. M. Balagurov, *Phys. Rev. B* **2009**, 80, 024409.

[13] H. Nakao, T. Murata, D. Bizen, Y. Murakami, K. Ohoyama, K. Yamada, S. Ishiwata, W. Kobayashi, I. Terasaki, *J. Phys. Soc. Jpn.* **2011**, 80, 023711.

[14] S. A. Chambers, T. C. Droubay, C. M. Wang, K. M. Rosso, S. M. Heald, D. A. Schwartz, K. R. Kittilstved, D. R. Gamelin, *Mater. Today* **2006**, 9, 28–35.; S. A. Wolf, D. D.

Awschalom, R. A. Buhrman, J. M. Daughton, S. von Molnár, M. L. Roukes, A. Y. Chtchelkanova, and D. M. Treger, *Science* **2001**, 294, 1488–1495.; M. Opel, *J. Phys. D: Appl. Phys.* **2012**, 45, 033001.

[15] D. Serrate, J. M. De Teresa, M. R. Ibarra, *J. Phys. Condens. Matter.* **2007**, 19, 023201.

[16] M. Hashisaka, D. Kan, A. Masuno, M. Takano, Y. Shimakawa, T. Terashima, K. Mibu, *Appl. Phys. Lett.* **2006**, 89, 032504.

[17] M. E. Flatté, G. Vignale, *Appl. Phys. Lett.* **2001**, 78, 1273.

[18] H.-U. Habermeier, *Mater. Today* **2007**, 10, 34–43.

[19] S. Fukushima, T. Sato, D. Akahoshi, H. Kuwahara, *J. Phys. Soc. Jpn.* **2009**, 78, 064706.

[20] A. M. Abakumov, H. D'Hondt, M. D. Rossell, A. A. Tsirlin, O. Gutnikova, D. S. Filimonov, W. Schnelle, H. Rosner, J. Hadermann, G. Van Tendeloo, E. V. Antipov, *J. Solid State Chem.* **2010**, 183, 2845–2854.

[21] The BM-structured $SrCoO_{2.5}$ is orthorhombic structure with space group *Ima*2, where the unit cell is defined as superstructure ($\sqrt{2}\,a \times \sqrt{2}\,a \times 4a$) from a primitive cell of the perovskite structure [A. Muñoz, C. de la Calle, J. A. Alonso, P. M. Botta, V. Pardo, D. Baldomir, J. Rivas, *Phys. Rev. B* **2008**, 78, 054404.].

[22] The unit cell of mixed-perovskite LSAT is generally defined as the double unit cell of primitive perovskite structure [D. Mateika, H. Kohler, H. Laudan, E. Völkel, *J. Cryst. Growth* **1991**, 109, 447.; D. A. Pawlak, M. Ito, L. Dobrzycki, K. Wozniak, M. Oku, K. Shimamura, T. Fukuda, *J. Mater. Res.* **2005**, 20, 3329.]. However, the diffraction peaks of LSAT substrate are denoted with asterisks in this study because there remains continued indexing issues related to the structure.

[23] S. Ishiwata, W. Kobayashi, I. Terasaki, K. Kato, M. Tanaka, *Phys. Rev. B* **2007**, 75, 220406.

[24] N. Ichikawa, M. Iwanowska, M. Kawai, C. Calers, W. Paulus, Y.Shimakawa, *Dalton Trans.* **2012**, 41, 10507.; H. Jeen, W. S. Choi, M. D. Biegalski, C. M. Folkman, I.-C. Tung, D. D. Fong, J. W. Freeland, D. Shin, H. Ohta, M. F. Chisholm, H. N. Lee, *Nature Mater.* **2013**, 12, 1057−1063.

[25] M. James, D. Cassidy, D. J. Goossens, R. L. Withers, *J. Solid State Chem.* **2004**, 177, 1886-1895.

[26] H. Ohta, H. Hosono, *Mater. Today* **2004**, 7, 42-51.

[27] Y. W. Long, N. Hayashi, T. Saito, M. Azuma, S. Muranaka, Y. Shimakawa, *Nature* **2009**, 458, 60–63.

[28] S. D. Findlay, N. Shibata, H. Sawada, E. Okunishi, Y. Kondo, T. Yamamoto, Y. Ikuhara, *Appl. Phys. Lett.* **2009**, 95, 191913.

[29] S. Yoshida, W. Kobayashi, T. Nakano, I. Terasaki, K. Matsubayashi, Y. Uwatoko, I. Grigoraviciute, M. Karppinen, H. Yamauchi, *J. Phys. Soc. Jpn.* **2009**, 78, 094711.

[30] N. F. Mott, *J. Non-Cryst. Solids* **1968**, 1, 1.; K. Yamaura, D. P. Young, R. J. Cava, *Phys. Rev. B* **2001**, 63, 064401.

[31] W. Koshibae, K. Tsutsui, S. Maekawa, *Phys. Rev. B* **2000**, 62, 6869–6872.

[32] H. Toyosaki, T. Fukumura, Y. Yamada, N. Nakajima, T. Chikyow, T. Hasegawa, H. Koinuma, M. Kawasaki, *Nature Mater.* **2004**, 3, 221–224.

[33] N. Nagaosa, J. Sinova, S. Onoda, A. H. MacDonald, N. P. Ong, *Rev. Mod. Phys.* **2010**, 82, 1539–1592.

[34] F. Matsukura, H. Ohno, T. Dietl, *Handbook of Magnetic Materials*, Elsevier, Amsterdam, **2002**, 14, 1–42.

[35] D. H. Kim, J. S. Yang, K. W. Lee, S. D. Bu, D.-W. Kim, T. W. Noh, S.-J. Oh, Y.-W. Kim, J.-S. Chung, H. Tanaka, H. Y. Lee, T. Kawai, J. Y. Won, S. H. Park, and J. C. Lee, *J. Appl. Phys.* **2003**, 93, 6125.

[36] T. Fukumura, H. Toyosaki, K. Ueno, M. Nakano, M. Kawasaki, *New J. Phys.* **2008**, 10, 055018.

[37] S. Onoda, N. Sugimoto, N. Nagaosa, *Phys. Rev. B* **2008**, 77, 165103.

[38] T. Fukumura, H. Toyosaki, K. Ueno, M. Nakano, T. Yamasaki, M. Kawasaki, *Jpn. J. Appl. Phys.* **2007**, 46, L642–L644.

[39] H. Ohta, Y. Sato, T. Kato, S. W. Kim, K. Nomura, Y. Ikuhara, H. Hosono, *Nature Commun.* **2010**, 1, 118.

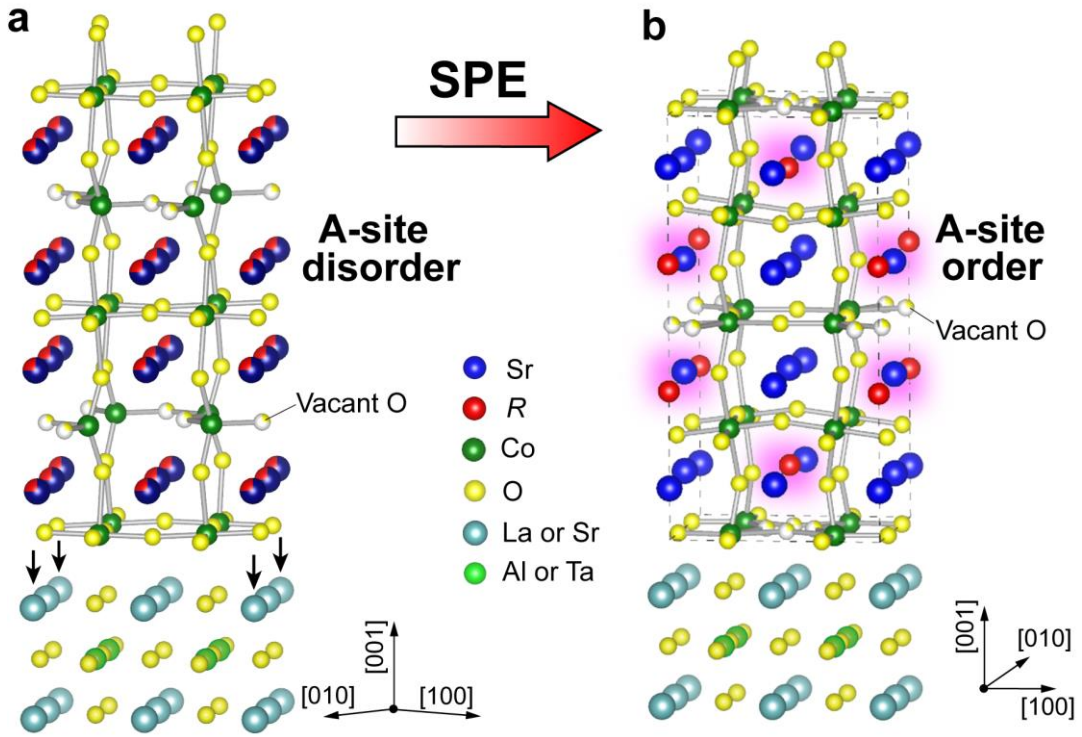

Figure 1. Schematic illustration of the strategy to produce epitaxial S*R*CO films with well-aligned A-site-ordered structure on (La,Sr)(Al,Ta)O_3 substrates; this was undertaken by solid-phase epitaxy (SPE) with two-step film-synthesis process combining low-*T* epitaxial growth and a subsequent high-*T* annealing. Here, the ideal crystal structure of A-site-ordered $Sr_3RCo_4O_{10.5}$ is shown. **(a)** the A-site-disordered perovskite framework of S*R*CO with oxygen-vacancy ordered structure (brownmillerite(BM)-type structure) is epitaxially grown on the substrates. **(b)** S*R*CO film with an A-site-ordered structure, obtained by high-*T* annealing of the as grown film with BM-type structure in air. The dashed line indicates the unit cell of A-site-ordered S*R*CO. In this study, Er was selected as element *R*. Crystalline orientations for as-grown [24] and SPE grown SECO films [7] are shown at the bottom right of each figure.

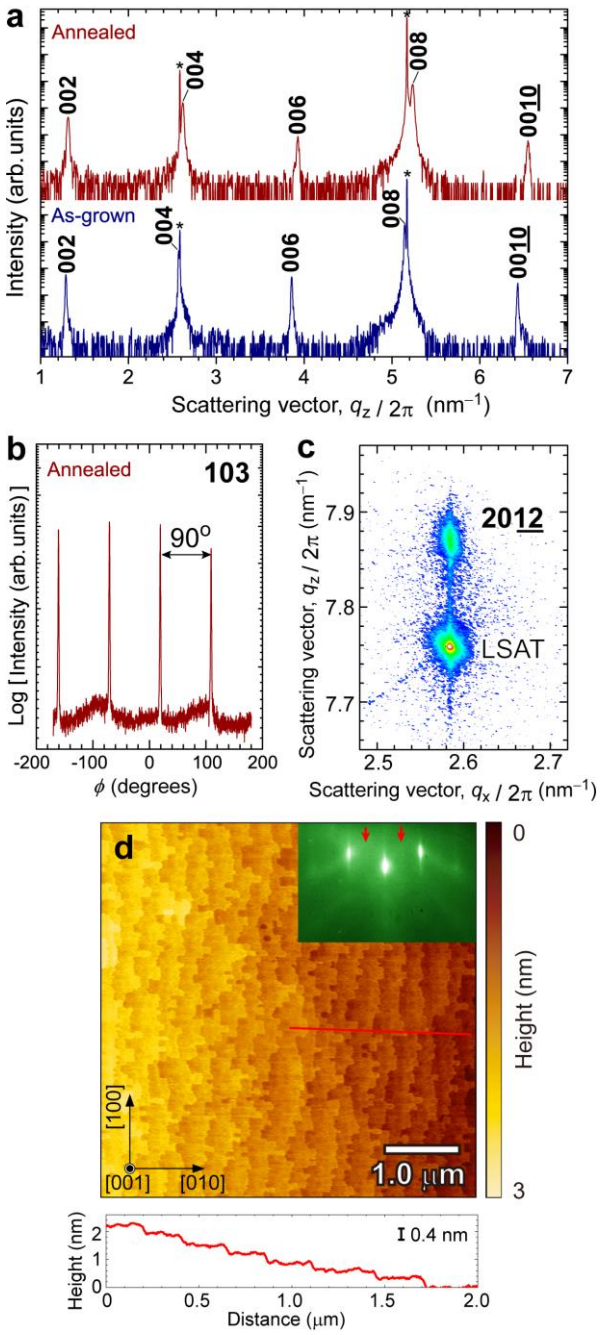

Figure 2. Structural characterization for SECO films as-grown (T_g = 820 °C, P_{O2} = 10 Pa) and SPE-grown (T_a = 1050 °C) at well-optimized conditions. **(a)** Out-of-plane XRD patterns of as-grown (blue) and SPE-grown (red) films. Diffraction indices are noted above the corresponding diffraction peaks. LSAT substrate peaks are indicated by asterisks (*). The double lattice spacing along the *c*-axis (l = 2, 6, 10) originates from the oxygen-vacancy ordering. **(b)** In-plane ϕ-scans for the asymmetric reflection of 103 diffraction peaks of the SPE-grown SECO films. The four diffraction peaks with 90° rotational intervals observed in the SPE-grown film are attributed to A-site ordering. **(c)** Reciprocal space mapping around 20$\underline{12}$ A-site-ordered SECO for the SPE-grown film. **(d)** Topographic AFM image of the SPE-grown SECO film. Below: Height profile derived from the red line on the image. Inset: RHEED pattern from this film, confirming the atomically flat surface of the SPE-grown SECO film. The arrows indicate the position of weak diffraction spots originating from the superstructure (A-site-ordered structure) of film surface and/or surface reconstruction.

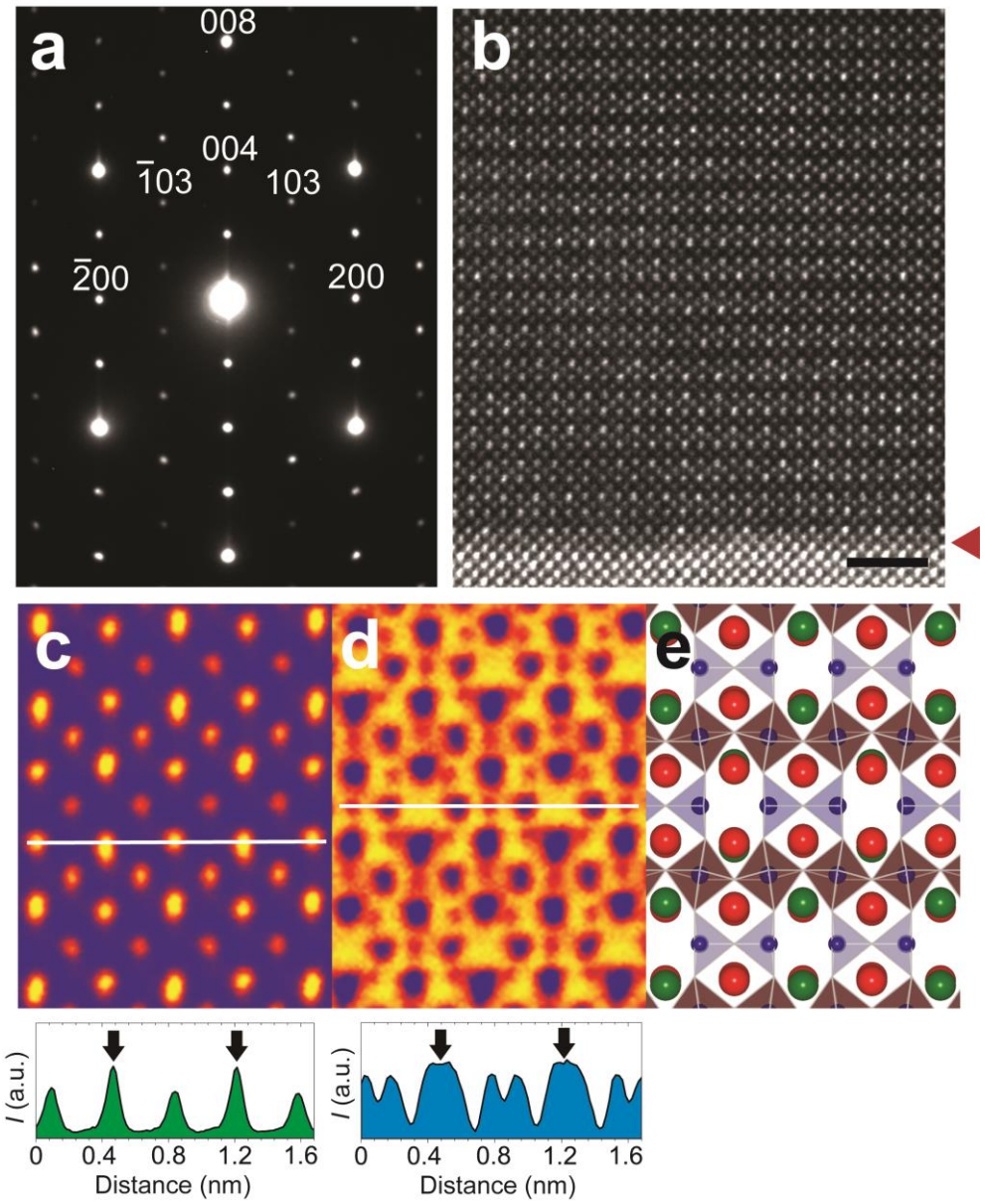

Figure 3. High-resolution STEM analyses of the SPE-grown SECO epitaxial films on LSAT substrates. **(a)** Selected-area electron diffraction pattern of the film with the main diffraction spots from SECO assigned. **(b)** Cross-sectional HAADF-STEM image (scale bar = 2 nm) — the red triangle denotes the position of the heterointerface. **(c)** Magnified HAADF-STEM and **(d)** ABF-STEM images, which are obtained by averaging 20 original HAADF and ABF images. These images are representative of the ordered structure observed in wide area of the SECO film. The bottom panels of (c) and (d) show HAADF and ABF intensity profiles, respectively, collected along the white lines in each image. The black arrows indicate the positions of Sr/Er columns and oxygen-vacancy columns in each panel. **(e)** A schematic illustration of the atomic structure of the ordered SECO.

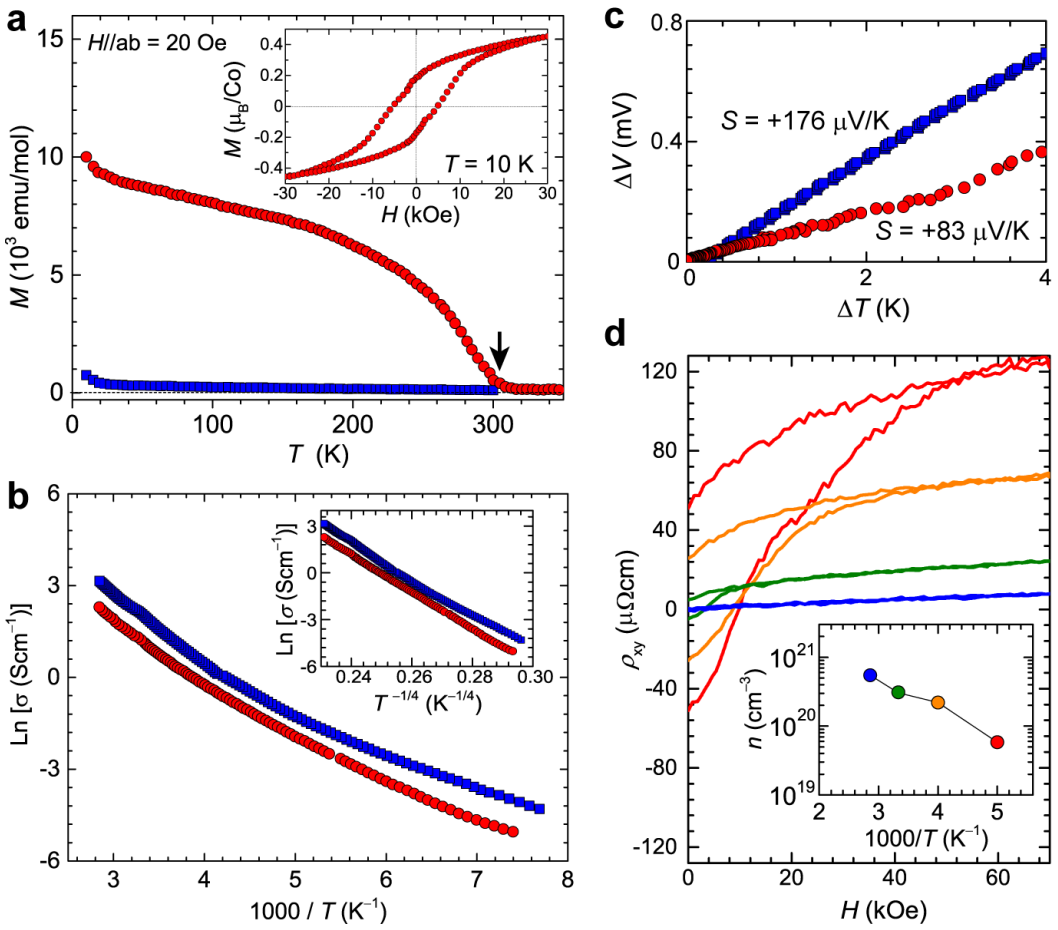

Figure 4. (**a**–**c**) Electromagnetic properties of SECO epitaxial films. Blue symbols: as-deposited, Red symbols: SPE-grown. **(a)** *M*–*T* curves measured under H = 20 Oe, applied parallel to in-plane direction. The arrow indicates the Curie temperature. The inset shows a magnetic hysteresis loop at 10 K for the SPE-grown SECO film. **(b)** σ–T plots. Inset: the linear relation between $\ln\sigma$ and $T^{-1/4}$, indicating that the charge carriers are localized at the entire temperature range. **(c)** ΔV–ΔT plots acquired at RT, demonstrating the p-type conductivity of SECO. The S-values obtained from the linear slope of ΔV–ΔT plots, shows a decrease from +176 μV K^{-1} to +83 μV K^{-1} after SPE-process. (d) H-dependence of ρ_{xy} for the SPE-grown SECO epitaxial film at 200 K (red), 250 K (orange), 300 K (green), and 350 K (blue). H is applied perpendicular to the film plane and the ρ_{xy} is derived from ½[$\rho_{xy}(+H)$ − $\rho_{xy}(-H)$]. Inset: T-dependence of carrier concentrations (n), estimated from the normal Hall coefficient.